Stromal Changes In The Aged Lung Induce An Emergence From Melanoma Dormancy

Ashani Weeraratna (aweeraratna@jhu.edu)
Johns Hopkins University https://orcid.org/0000-0003-0448-6952
Mitchell Fane
Johns Hopkins
Stephen Douglass
Johns Hopkins
Gretchen Alicea
Johns Hopkins
Marie Webster
Lankenau Institute of Medical Research
Vito Rebecca
Johns Hopkins
Gloria Marino
Johns Hopkins
Yash Chhabra
Johns Hopkins
Filipe Almeida
Wistar Institute
Brett Ecker
The Wistar Institute
Thomas Beer
Wistar Institute
Hsin-Yao Tang
Wistar Institute
Andrew Kossenkov
Wistar Institute
David Speicher
Wistar Institute
Julio Aguirre-Ghiso
Icahn School of Medicine at Mount Sinai

Research Article

Keywords:

Posted Date: September 16th, 2020

DOI: https://doi.org/10.21203/rs.3.rs-61165/v1

Version of Record: A version of this preprint was published at Nature on June 1st, 2022. See the published version at https://doi.org/10.1038/s41586-022-04774-2.

Abstract

Dormant tumor cells escape the primary site, do not grow out into macroscopic tumors in the distal site, but maintain enough plasticity to reactivate and form overt metastatic lesions, sometimes taking several decades. Despite its importance in metastasis and residual disease, few studies have been able to successfully model or characterize dormancy within melanoma. Here, we show that age-related changes in the lung microenvironment facilitate a permissive niche for efficient outgrowth of disseminated dormant tumor cells, in contrast to the aged skin, where age-related changes suppress melanoma growth but drive dissemination. A model of melanoma progression that addresses these microenvironmental complexities is the phenotype switching model, which argues that melanoma cells switch between a proliferative cell state and a slower-cycling, invasive state[1–3]. Dermal fibroblasts are key orchestrators of promoting phenotype switching in melanoma via changes in the secretion of soluble factors during aging[4–8]. Specifically, we have identified Wnt5A as a master regulator of activating metastatic dormancy, which enables efficient seeding and survival of melanoma cells in metastatic niches. Age-induced reprogramming of lung fibroblasts increases their secretion of the soluble Wnt antagonist sFRP1, which inhibits Wnt5A, enabling efficient metastatic outgrowth. Further, we have identified the tyrosine kinase receptors AXL and MER as promoting a dormancy-to-reactivation axis respectively. Overall, we find that age-induced changes in distal metastatic microenvironments promotes efficient reactivation of dormant melanoma cells in the lung.

Main

We have previously established that melanoma cells implanted in aged mouse skin metastasize to the lung at greater rates than in younger animals[4]. Whether this is due to increased dissemination from the primary site, or because the aged microenvironment at metastatic sites promotes outgrowth remained unclear. To investigate this, we intradermally implanted Yumm1.7 (mCherry) melanoma cells into young (8 weeks) and aged (> 52 weeks) C57BL6 mice. The primary tumor in the skin grew faster in young mice (Fig. 1A). We examined distal lung metastases at weeks 1, 3 and 5 using immunohistochemical (IHC) analysis of mCherry positive cells in the lung. At week 1, we failed to detect melanoma cells. At week 3, we found that melanoma cells efficiently seed the lung in equal numbers in young and aged mice (Fig. 1B) as single cell colonies (Fig. 1C, top panels); however, at week 5, larger metastatic colonies formed in the aged lung (Fig. 1C, bottom right), while cells persisted as single cells in the young (Fig. 1C, bottom left). While the number of cells that seeded in the young vs. aged lung are similar, the rate at which cells seed the lung (no. of cells disseminating/mm^3 of tumor volume) was far lower in young mice. Thus, to determine whether the difference in lung outgrowth at week 5 was due to an overall increase in dissemination from aged primary tumors, we removed the primary tumors from aged mice after initial dissemination and seeding (3 weeks) to prevent further dissemination. This did not affect the rate of metastatic outgrowth (Extended Data 1A), suggesting that after an initial period of single-cell dissemination and seeding, the *aged* lung microenvironment promotes proliferation of single cells, allowing melanoma outgrowth, whereas the *young* lung suppresses growth. Interestingly, these changes

contrast to those previously observed in the skin, where the aged skin microenvironment *decreased* melanoma growth (Fig. 1A), while promoting local invasion[4].

Given our previous data on skin fibroblasts driving changes in melanoma cell behavior[4], we investigated whether lung fibroblasts similarly affected melanoma cell growth at the distal sites. We co-cultured melanoma cells with human skin or lung fibroblasts from young (< 35 years) or aged (> 55 years) healthy donors in a 3D collagen reconstruct (Fig. 1D-E, Extended Data 1B-D). Consistent with our *in vivo* data (Fig. 1A-C), melanoma cells in an aged lung fibroblast microenvironment increased proliferation compared to those in a young lung fibroblast environment (Fig. 1D-E, Extended Data 1B-D). Conversely, melanoma cells in an aged skin fibroblast microenvironment proliferated more slowly when compared with young skin fibroblasts. Importantly, treatment of human melanoma cells (Fig. 1F-G, Extended Data 2A-F) with conditioned media (CM) from young and aged lung or skin fibroblasts over a 10-day period in 2D culture phenocopied the results seen in 3D culture, suggesting that changes in secreted soluble factors are key in promoting these phenotypic differences.

Since aged lung fibroblasts induced melanoma cell proliferation *in vitro* (Fig. 1D-G), we performed proteomic analysis on the secretome from healthy human young (< 35) and aged (> 55) lung fibroblasts (Fig. 1H). One of the most differentially secreted factors increased in the aged lung fibroblast secretome was sFRP1, a non-canonical Wnt antagonist[9–11]. This was intriguing, as previous analyses in aged *skin* fibroblasts revealed increased secretion of sFRP2, DKK3 and Wnt5A, which conversely promoted expression of the non-canonical Wnt signaling pathway in tumor cells, which was shown to be a prominent driver of a slower-growing, but invasive melanoma phenotype within primary tumors[4–6,12]. Analysis of primary tumor lysate from young and aged mice in this study confirmed that indeed, aged mouse tumors have increased expression of the main effector protein in the non-canonical Wnt pathway, Wnt5A (Fig. 1I). Downstream pathways of Wnt5A signaling in melanoma, such as AXL[13] and slow-cycling genes such as p21 and p27, were all increased in aged tumors in the skin (Fig. 1I). Conversely, well known targets of the proliferative axis within melanoma phenotype switching such as β-catenin, MITF and MART-1[3], along with lesser known proliferative melanoma-associated markers including MER[14] and H2AFZ[15], are all decreased in aged skin tumors (Fig. 1J), coinciding with the overall increased growth seen in these younger tumors (Fig. 1A). A recent observation within prostate cancer revealed that invasive pathways such as Wnt5A[16] and AXL[17] independently promote tumor cell dormancy, and potentially, survival within metastatic bone microenvironments following dissemination[18]. Subsequently, we analyzed other well-defined markers of tumor dormancy in prostate and other cancer types, such as NR2F1, p-p38 and TGFB2[17,19]. All were increased in Wnt5A/AXL^{high} slower-growing aged primary tumors in the skin (Fig. 1I), implicating Wnt5A and AXL in age-related signaling changes in melanoma dormancy.

Taken together, while our previous data suggested that sFRP2 within the aged *skin* promotes non-canonical Wnt signaling to allow initial dissemination from the primary tumor[4], this current data suggested that sFRP1 within the aged *lung* inhibits Wnt5A to induce reactivation and metastatic outgrowth after an initial period of dormancy. To test this hypothesis, we treated human melanoma cells

with CM from 3 young or aged healthy human lung fibroblast donors. Treatment with aged lung fibroblast CM consistently reduced non-canonical Wnt5A signaling compared with young lung fibroblasts (Fig. 2A, Extended Data 2G). Downstream dormancy associated pathways were also reduced, while proliferative pathways were increased (Fig. 2A Supp 2G). Conversely, treatment with CM from aged *skin* fibroblasts induced the opposite effect on gene expression, promoting non-canonical Wnt5A/downstream dormancy pathways while inhibiting proliferative pathways (Fig. 2B, Extended Data 2H). Next, we treated melanoma cells with recombinant (r) sFRP1; we observed decreased Wnt5A and downstream dormancy markers AXL and p21, and increased proliferative markers MITF and MER (Fig. 2C, Extended Data 3A), as well as increased proliferation (Fig. 2D, Extended Data 3B). Furthermore, knockdown of sFRP1 from aged lung fibroblasts (Fig. 2E) ablated the previous growth phenotype and decreased proliferation of melanoma cells treated with CM relative to empty control (Fig. 2F, Extended Data 3C). To test this hypothesis in vivo, we intradermally injected aged mice with Yumm1.7 mCherry cells to form primary tumors. Tumors were grown for 3 weeks to allow single cell seeding within the lung, as shown in Fig. 1C, then treated with a neutralizing antibody against sFRP1 via Intraperitoneal (IP) injections to deplete its levels within the mouse until week 5. Depletion of sFRP1 reduced metastatic colony formation in the aged lungs compared with IgG treated mice (Fig. 2G-H). Overall, we find that aged lung fibroblasts promote phenotypic reactivation of dormant melanoma cells in the lung via increased secretion of sFRP1 (Fig. 2I).

Given the importance of Wnt5A in prostate cancer dormancy[16], coupled with it being a downstream antagonistic target of sFRP1, we chose to investigate it as a primary factor in melanoma dormancy. We first stratified patient melanoma samples (across both primary and metastatic) from the TCGA into the top and bottom 25th percentile of Wnt5A-expressing primary and metastatic tumors. Wnt5A high-expressing patient samples express a large number of well-defined dormancy related genes[20–22] (Fig. 3A). Importantly, many established proliferative melanoma markers correlated with Wnt5A^{low} samples (Fig. 3B). Increasing Wnt5A expression in low-expressing human melanoma cells via lentiviral overexpression (Fig. 3C, Extended Data 4D) or treatment with rWnt5A (Extended Data 4I) increased many of these dormancy targets, while reducing proliferative markers and melanoma cell growth *in vitro* (Extended Data 4E-G) .

We next investigated whether Wnt5A expression promotes non-progressive, dormant disease in metastatic patients. We evaluated the TCGA dataset, first looking at progression free interval (PFI) in metastatic patients only. We stratified patients into those who progressed in < 3 years vs in > 3 years. Patients who progressed in < 3 years were significantly older (Fig. 3D). Importantly, Wnt5A expression in metastatic samples was significantly higher in the younger patient cohort with progression in > 3 years (Fig. 3E). Analysis of these data via Kaplan Meier curves further shows that overall PFI probability is significantly higher in younger metastatic patients with lower Wnt5A levels (Extended Data 4A-B). Examination of overall survival further shows that metastatic patients who did not survive up to 3 years were also significantly older (Fig. 3F) and had lower Wnt5A expression in metastatic sites (Fig. 3G). Overall survival probability significantly decreases in both aged patients and lower Wnt5A expression in metastatic samples (Fig. 3H). This was in direct contrast to our analysis of Wnt5A expression in patient

primary tumors, which showed the opposite outcome, with higher Wnt5A expression within these primary tumors correlating with worst survival (Extended Data 4C). This speaks to the complexity of Wnt5A signaling within these different microenvironments and in the overall metastatic cascade. While our previous studies implicate the importance of Wnt5A in establishing an invasive phenotype[23], dissemination[5], and in therapeutic resistance[24] within the primary tumors, these new data suggested that in order to form competent, proliferative metastases at the distal site, Wnt5A needs to be down-regulated. This is further supported by the fact that Wnt5A expression is reduced in established metastatic tumor sites vs primary tumors in the TCGA (Fig. 3I) and other independent patient datasets (GSE15605)[25] (Extended Data 4H).

To investigate this further, we generated Yumm1.7 mCherry Doxycycline (Dox) inducible cells that expressed sh-Wnt5A. Treatment with Dox (Dox, 0.5ug/ml) successfully reduced Wnt5A expression, while reducing downstream dormancy markers, increasing proliferative markers and overall proliferation (Fig. 3J-K). We were interested in how uncoupling of Wnt5A across different timepoints in progression affected dissemination and metastatic dormancy. We formed intradermal tumors in our young c57BL6 mouse model, which were able to disseminate to the lungs efficiently but maintained dormant cell colonies in the lungs through week 5 (see Fig. 1C). We specifically investigated temporal downregulation of Wnt5A starting at two different timepoints; 1) Beginning at day 3, to investigate Wnt5A ablation throughout the entirety of tumor progression (growth and dissemination) and; 2) Beginning at day 21, to investigate Wnt5A downregulation after cells had successfully disseminated and formed viable single dormant colonies within the lung (See Fig. 1C). Analysis of primary tumor growth reveals that inducible knockdown at either timepoint significantly increased overall growth (Fig. 3L), further establishing a role for Wnt5A in inducing a slower-growing cell within primary tumors. However, analysis of metastatic progression after 5 weeks revealed that only mice treated with Dox starting at day 21 formed large micrometastatic colonies, compared with non-treated mice, who predominantly contained single dormant cells (Fig. 3M, O). Interestingly, inducible knockdown of Wnt5A beginning at day 3 resulted in significantly fewer cells seeded in the lung compared with no-Dox treated mice (Fig. 3N). Overall, these new data demonstrate that non-canonical Wnt5A signaling is required for efficient dissemination from the primary tumor, and survival when seeding within the lung initially. Once these cells have successfully seeded as viable single dormant cells, temporal down-regulation of Wnt5A is able to promote reactivation, allowing metastatic outgrowth, even in the previously dormant young mouse lungs (Fig. 3P).

To further investigate the mechanisms underlying the complexity of dormancy vs outgrowth in aging, we next investigated the Tyro3, AXL and MER (TAM) family of tyrosine kinase receptors. Importantly, AXL is strongly correlated positively to Wnt5A in melanoma[26] and is involved in driving dormancy in metastatic prostate cancer[17]. The relationship between AXL with the other family members is very context specific, as all three members are heavily co-expressed within immune cells and act in a redundant manner[27]. Conversly in melanoma, both MER and TYRO3 have been suggested to be differentially expressed to AXL and promote more of a proliferative phenotype[14,28]. Thus, we hypothesized that differential expression of AXL vs either MER or TYRO3 within melanoma cells may act to promote a dormancy-reactivation axis

within metastatic tissues. To investigate this, we performed westernblot analysis of 3 previously characterized Wnt5A^{high} human melanoma cell lines (FS4, FS5, 1205LU) vs 2 characterized Wnt5A^{low} cell lines (FS13, FS14) (Fig. 4A). AXL strongly correlated positively with Wnt5A and these cells expressed the AXL ligand GAS6. Several established dormancy markers including p21, phospho-p38, and NR2F1 were also elevated in these Wnt5A/AXL^{high} cells (Fig. 4A). While there was no consistent difference seen in TYRO3 expression across the cell lines, MER was inversely expressed with AXL and Wnt5A. These MER^{high} expressing cell lines also displayed strong expression of the MER-specific ligand PROS1 and the proliferative markers MITF, and MART1 (Fig. 4A).

To expand on this analysis in melanoma cells specifically, we analyzed an RNA-seq dataset from the Cancer Cell Line Encyclopedia (CCLE) that contains over 60 human melanoma cell lines. We stratified these into AXL^{high} and AXL^{low} subpopulations. Indeed, AXL^{high} cells have significantly elevated levels of Wnt5A and dormancy markers (Fig. 4B), reduced expression of melanoma proliferative markers (Fig. 4C), and low MER expression. Subsequent stratification and analysis of MER^{high} and MER^{low} expressing cell lines from within this dataset reveals the opposite trend, in that Wnt5A, AXL, and dormancy markers are reduced in MER^{high} cells (Fig. 4D) while proliferative markers are markedly increased (Fig. 4E). Knockdown of AXL in Wnt5A^{high} lines did not reduce Wnt5A, suggesting that AXL may be downstream of Wnt5A within this dormancy axis; however, MER and MITF were increased (Fig. 4G) alongside a modest increase in proliferation after 10 days (Fig. 4F). Conversely, shRNA-mediated knockdown of MER increased Wnt5A, AXL, and p21 expression, while reducing MITF (Fig. 4I, Extended Data 5A) and proliferation (Fig. 4H, Extended Data 5B). Given that MER knockdown increased Wnt5A/AXL signaling and proliferation, we hypothesized that MER promotes reactivation from metastatic dormancy. To investigate this, we created a Dox-inducible Yumm1.7 mCherry MER melanoma cell line. Inducible overexpression of MER decreased AXL and Wnt5A, while increasing MITF (Fig. 4K) and overall proliferation *in vitro* (Fig. 4J). Further validation of MER playing an important role in metastatic outgrowth came via analysis of the TCGA and other independent patient studies (GSE15605)[25]. MER expression was significantly increased in metastatic patient samples compared to primary tumors in both datasets (Fig. 4L, Extended Data 5C) and was also increased in patients with stage III/IV disease relative to stage I/II (Extended Data 5D), suggesting an importance for driving metastatic growth and progression.

To investigate MER expression in metastatic reactivation *in vivo*, we used the Dox-inducible MER overexpressing Yumm1.7 mCherry cell line. These cells were implanted intradermally into our dormant young mouse model to form primary tumors. We again began treatment with Dox at either day 3 or day 21 to investigate the importance of MER expression at various timepoints throughout progression. Dox treatment at both timepoints increased overall tumor growth (Fig. 4M), confirming that MER expression promotes a more proliferative phenotype. Induction of MER expression in dormant single cells seeded within the lung (starting at day 21) significantly increased metastatic outgrowth compared with non-treated mice, where cells remained largely as single dormant colonies (Fig. 4N-O). MER induction beginning at day 3 decreased the number of cells able to seed (Fig. 4N), further highlighting the necessity

for a Wnt5A^{high}/MER^{low} melanoma phenotype during early tumor development to allow dissemination from the primary tumor and survival during metastatic seeding (Fig. 3P).

We next created a Dox-inducible AXL mCherry Yumm1.7 melanoma cell line to investigate whether AXL could inhibit reactivation via inhibition of this MER phenotypic switch within metastatic aged models. Indeed, inducible activation of AXL in these cells decreased MER and MITF expression (Fig. 4P) as well as proliferation *in vitro* (Extended Data 5E); however, Wnt5A remained unchanged, further implicating AXL downstream of Wnt5A in this dormancy axis. AXL-inducible cells were implanted in the aged metastatic mouse model to form primary tumors and treated with Dox beginning at either day 3 or day 21. This aged mouse model has slow-growing primary tumors with higher AXL expression relative to younger mice under normal circusmtances (Fig. 1). Despite the already high level of AXL within these tumors, AXL induction was able to produce a modest decrease in tumor growth, but only upon treatment starting at day 3 (Fig. 4Q). AXL induction at days 3 and 21 significantly reduced colony formation in the aged lung and largely resulted in single cell colonies compared to the no Dox control (Fig. 4R-S). There was no difference in colony formation size between AXL induction at day 3 and 21, which we hypothesized was due to the fact that AXL expression is already higher in aged primary tumors, thus already allowing efficient dissemination and survival upon seeding. Overall, this data suggests a key role for this AXL/MER differentially regulated signaling pathway in producing a dormancy/reactivation axis downstream of Wnt5A.

Finally, we were interested in whether activation of this differential TAM axis by their respective primary ligands played a role in both dormancy and reactivation. GAS6 is the prominent ligand involved in activating AXL, although it has been shown to bind both MER and TYRO3 at a much lower affinity[29]. PROS1 is the prominent ligand for MER, but appears to be much more specific compared to GAS6, and is unable to bind the AXL receptor in most contexts[30,31]. Analysis of ligand expression in the healthy lungs of young mice, which promote a dormant melanoma phenotype, reveals that GAS6 levels appeared to be higher in the majority of younger mouse lungs. Conversely, PROS1 levels were increased in the aged lung (Fig. 5A). Furthermore, we find that Wnt5A/AXL^{high} cells secrete higher amounts of the GAS6 ligand into conditioned media *in vitro*, whereas MER^{high} cells secrete higher amounts of PROS1, implicating the potential for paracrine-related modulation of neighboring melanoma cells in the microenvironment (Fig. 5B).

Treatment of Wnt5A/AXL^{high} melanoma cells with rGAS6 consistently decreased melanoma cell proliferation across these cell lines (Fig. 5C, Extended Data 6A). However, Wnt5A/AXL^{low} melanoma cells treated with GAS6 increased proliferation (Fig. 5D, Extended Data 6B). We hypothesized, given GAS6's promiscuity between the 3 different TAM family members, that it may actually be acting through the MER receptor in AXL^{low} cell lines. Indeed, shRNA knockdown of MER in AXL^{low} human melanoma cells, which increased AXL in previous experiments, instead decreased melanoma cell proliferation in response to rGAS6 treatment (Extended Data Fig. 6C); Conversely, sh-mediated knockdown of AXL in Wnt5A/AXL^{high} cells treated with rGAS6 recues the phenotype and reverses the decreased proliferative response

(Extended Data Fig. 6D). Treatment of Dox-inducible AXL melanoma cells upon AXL induction with rGAS6 decreased melanoma cell growth compared with untreated AXL-induced cells or with rGAS6 treatment in control cells (Fig. 5E). Protein expression analysis of these cells confirms that rGAS6 treatment of Yumm1.7 cells produces only a modest decrease in MER and MITF and a slight increase in Wnt5A (Fig. 5F). When AXL expression is induced via Dox treatment, administration of rGAS6 increases Wnt5A and produces a much more pronounced decrease in MER and MITF, suggesting that GAS6 regulation of melanoma cells relies heavily on whether they are in an AXL- or MER-high state. To investigate this *in vivo*, we formed primary tumors in our aged metastatic mouse model that had lower GAS6 levels in the lung. We began treatment of these mice with rGAS6 (IP injection) at 3 weeks to allow initial dissemination and seeding in the lung (Fig. 1C). We found that GAS6 treatment decreased metastatic colony formation after 5 weeks (Fig. 5G-H); however, this decrease was modest and larger micrometastatic colonies were still found in treated mice, as opposed to single cell colonies seen previously within the young lung. These data suggested that GAS6 is unable to fully inhibit the phenotypic switch towards reactivation in the aged lung microenvironment, likely due to competion with other soluble factors such as sFRP1.

While GAS6 shows promiscuous regulation of cell growth based on the adopted cell phenotype, PROS1 is thought to have very little receptor interaction with AXL. We showed previously that even in Wnt5A/AXL^{high} melanoma cell lines *in vitro*, MER expression was still maintained at detectable levels (Fig. 4A). Based on this, we hypothesized that PROS1 may act to specifically promote increased growth and reactivation regardless of cell phenotype. Indeed, treatment of either Wnt5A/AXL^{high} or MER^{high} human and mouse melanoma cells significantly increased melanoma growth (Fig. 5J, Extended Data 6E-H); shRNA mediated knockdown of MER ablates this effect (Extended Data 6I). Protein expression analysis of rPROS1 treated Yumm1.7 cells shows that not only did PROS1 decrease Wnt5A and AXL expression, but further increased MER and MITF (Fig. 5I). To examine whether the PROS1 ligand could facilitate reactivation of dormant melanoma cells within our dormant young mouse model where PROS1 levels were low in the lung, we implanted primary tumors in young mice using Yumm 1.7 mCherry cells. Tumors were grown for 3 weeks to allow single cell seeding in the lung (see Fig. 1C). Mice were then treated with r-PROS1 every two days via IP. Treatment with r-PROS1 significantly increased metastatic colonies in the previously dormant young lung microenvironment at 5 weeks, compared with a PBS control (Fig. 5K,L).

Overall, these data reveal an unexpected complexity in the role of Wnt signaling in melanoma cell metastasis that is regulated by aging (Fig. 5M). We show that Wnt5A promotes initial dissemination of the tumor cells as previously defined, but then acts to maintain them in a dormant state to allow survival and adaptation in the lung microenvironment. This state is maintained until age-related changes in the distal site microenvironment induce an emergence from tumor dormancy. We specifically show that sFRP1 is secreted at higher levels by aged-lung fibroblasts and decreases Wnt5A expression to allow reactivation from dormancy in the aged mouse lung. We further define an AXL-MER dormancy-reactivation axis downstream of Wnt5A. MER expression is required to induce a phenotypic downregulation of the Wnt5A/AXL^{high} dormant state to allow age-induced metastatic reactivation and

outgrowth, whereas maintaining AXL expression inhibits reactivation. While we find that GAS6-mediated regulation of this axis is promiscuous, the MER-mediated ligand PROS1 is increased in the aged lung microenvironment and secreted in a paracrine manner by MER^{high} reactivated cells and is shown to be capable of driving reactivation and metastatic outgrowth in the previously dormant young lung microenvironment (Fig. 5M). These observations may explain the predisposition of elderly patients to aggressive metastatic melanoma and identify the role of aging as a critical step in in the emergence of tumor cells from dormancy. Further, these data, and other data from our laboratory and others suggest that treating patients according to age may have benefit. For example, we have recently shown that lipid uptake by melanoma cells in an aged, but not young, microenvironment drives resistance to BRAF/MEK inhibitors, which can be overcome by targeting the fatty acid transporter (FATP2) responsible[8]. Gomes et al have similarly shown that the accumulation of methylmalonic acid can drive tumor progression during aging[32]. Taken together, all of these data strongly suggest that we need to consider age as a parameter in the design and delivery of cancer therapy, and in the study of tumor dormancy and progression.

Methods

Cell Culture

FS4, FS5, FS13 and FS14 melanoma cells were maintained in RPMI (Invitrogen), supplemented with 10% FBS, and 100 units per millilitre penicillin and streptomycin. 1205Lu cells were maintained in MCDB153 (Sigma)/L-15 (Cellgro) (4:1 ratio) supplemented with 2% FBS and 1.6 mM CaCl2 (tumour growth media). YUMM1.7 murine cultured melanoma cells were maintained in DMEM F-12 (HEPES/glutamine) supplemented with 10% FBS, and 100 units per milliliter penicillin and streptomycin. Dermal fibroblast cell lines were obtained from Biobank at Coriell Institute for Medical Research and from Donors via the Baltimore Longitudinal Study of Aging and lung fibroblasts were purchased from ATCC and Coriell. Fibroblasts were maintained in DMEM, supplemented with 10% FBS, 100 units per millilitre penicillin and streptomycin. Cell lines were cultured at 37°C in 5% CO_2 and the medium was replaced as required. Cell stocks were fingerprinted using an AmpFLSTR Identifiler PCR Amplification Kit from Life Technologies at The Wistar Institute Genomics Facility. Although it is desirable to compare the profile with the tissue or patient of origin, our cell lines were established over the course of 40 years, long before acquisition of normal control DNA was routinely performed. However, each short tandem repeat profile is compared with our internal database of over 200 melanoma cell lines, as well as control lines, such as HeLa and 293T. Short tandem repeat profiles are available upon request. Cell culture supernatants were tested for mycoplasma using a Lonza MycoAlert assay at the University of Pennsylvania Cell Center Services.

Proliferation Assays

$2x10^4$ melanoma cells were seeded into a six well plate in triplicate. Cells were then counted at days 3, 5 and 10 post-seeding using a haemocytometer and NIS elements automated software. The total number of cells were analyzed using GraphPad Prism software, presented as the mean +/- the SEM. The 3D reconstruct proliferation assay was performed by seeding young or aged fibroblasts into a top and

bottom collagen layer (collagen I, Gibco A1048301) and GFP melanoma cells in a middle layer at a density of $2x10^5$ in a 24 well plate. The cells were imaged using the Nikon TE automated microscope and cell number per field was quantified using NIS elements, with the data represented in GraphPad Prism as the mean +/- the SEM.

Western Blot

Cell lines were plated and lysed with RIPA buffer supplemented with protease and phosphatase inhibitors. Total protein lysate was quantified using a Pierce™ BCA assay kit (# 23225, Thermo Fisher Scientific) and 50mg of protein was prepared in sample buffer, heated and loaded into NuPAGE™ 4-12% Bis-Tris Protein Gels (#NP0321BOX, Thermo Fisher Scientific) and ran at 160 volts. Proteins were then transferred onto PVDF membrane using the iBlot system (Invitrogen), and blocked in 5% milk/TBST for 1 hour. Primary antibodies were diluted in 5% milk/TBST and incubated at 4°C overnight. The membranes were washed in TBST and probed with the corresponding HRP-conjugated secondary antibody at 0.2µg/ml. Proteins were visualized using, ECL prime (Amersham, Uppsala, Sweden) and detected using ImageQuant™ LAS 4000 (GE Healthcare Life Sciences, Pittsburgh, PA).

Antibodies:

Antibodies were purchased from the following commercial vendors and used at the indicated dilutions for western blot: GAPDH (1:10,000, Cell Signaling #2118S), HSP90 (1:10,000, Cell Signaling #4877S), human AXL (1:1000, Cell Signaling #8661S), human MER (1:1000, Cell Signaling #4319), p21 (1:1000, Cell Signaling #2947), p27 (1:1000, Cell Signaling #3686S), Coup TFI/NR2F1 (1:1000, Cell Signaling #6364S), phosphor-p38 (1:500, Cell Signaling #9211S), H2AFZ (1:1000, Cell Signaling #2718S), MITF (1:1000, Cell Signaling #12590), human GAS6 (1:1000, Cell Signaling #67202S), human PROS1 (1:1000, R & D Systems #AF4036), Wnt5A (1:50, R & D systems biotin labeled, #BAF645), mouse AXL (1:1000, R & D Systems #AF854), mouse MER (1:1000, R & D Systems #MAB591-100), mouse p21 (1:1000, Abcam #ab188224), MART1 (1:1000, Thermo Scientific #MS716P0), β-Catenin (1:1000, Cell Signaling #8814S), TGFβ2 (1:500, Abcam #ab36495), mouse GAS6 (1:1000, R & D Systems #MABAF986) and mouse PROS1 (1:1000, R & D Systems #4976). Antibodies used for IHC were mCherry (1:200, Novus Biological #NBP2-25157). Neutralizing antibodies used in *in vivo* experiments were α-sFRP1 (1mg/kg, Sigma Aldrich ABS1593) and IgG control (1mg/kg, R & D Systems AB-105-C).

shRNA, lentiviral production and infection

MER, AXL and sFRP1 shRNA was obtained from the TRC shRNA library available at The Wistar Institute (TRCN0000000865, TRCN0000000862, TRCN0000000572, TRCN0000000573 TRCN0000062170 and TRCN0000062171). The Doxycycline-inducible on system (Tet3g vector: pLV[Exp]-EGFP:T2A:Puro-EF1A>Tet3G VB190411-1425qrz) was sourced from vector builder while the plasmid used for the inducible MER component was a pLV-mCherry-TRE3GMER cloned vector and the AXL component was a PLV-mCherry-TRE3GAXL cloned vector. The mCherry (pLV[Exp]-Bsd-EF1A>mCherry, VB180821-1150kqt) and GFP (pLV[Exp]-Puro-EF1A>EmGFP, VB171103-1159dvu) were purchased from vector builder. The

Doxycycline shRNA Wnt5A (Clone Id: V2THS_172016) TRIPZ system was purchased from Dharmacon. The Wnt5A overexpression cells was driven by the cloned vector pLU-EF1Wnt5A-iCherry. Lentiviral production was performed according to the protocol suggested by the Broad Institute. Briefly, 293T cells were at 70% confluency and co-transfected with shRNA plasmid and the lentiviral packaging plasmids (pCMV-dR8.74psPAX2, pMD2.G for 2^{nd} generation, pMDLg/pRRE, pRSV/REV and PMD2.G for 3^{rd} generation). Appropriate empty vector and scrambled controls were created for Overexpressing and shRNA constructs respectively. Cells were transduced with lentivirus for 48 hours, and then treated with appropriate antibiotic selection (puro, hygro, blast) with previously established kill curves for each cell line or were sorted for their selection marker (mCherry or GFP).

In-vivo allograft assays

All animal experiments were approved by the Institutional Animal Care and Use Committee (IACUC) (IACUC #112503X_0 #112510X_0 and M019h421) and were performed in an Association for the Assessment and Accreditation of Laboratory Animal Care (AAALAC) accredited facility.

Young *vs.* aged animal experiments: YUMM1.7 murine melanoma cells (2.5×10^5) overexpressing mCherry were injected subdermally into aged (>300 days old) and young (6-8 weeks old) c57BL6 mice (Charles River). Tumors were allowed to grow for a period of 1, 3 and 5 weeks for appropriate experiments. Neutralizing sFRP1 experiments: YUMM1.7 murine melanoma cells (2.5×10^5) expressing mCherry were injected subdermally into aged mice. After 3 weeks of tumor growth, mice were IP injected with α-sFRP1 or an IgG control at a concentration of 1mg/kg every 4 days until 5 weeks of total tumor growth. Dox-inducible sh-Wnt5A, MER and AXL Dox experiments: YUMM1.7 (mCherry) murine melanoma cells (2.5×10^5) transduced with a lentiviral TRIPZ Dox-inducible sh-Wnt5A vector or a MER/AXL Dox-inducible vector were injected subdermally into young (8 week old) C57/BL6 mice (Charles River). Expression of these vectors was controlled by administration of doxycycline (2mg/kg in the water) and was given at day 3 or day 21 of tumor growth. Recombinant protein treatments: YUMM1.7 (mCherry) murine melanoma cells (2.5×10^5) were injected subdermally into young (6-8 week old) c57BL6 mice (Charles River). After 3 weeks of growth, mice were IP injected with 200ng of r-PROS1 (R & D systems, 9740-PS), 200ng of r-GAS6 (R & D systems, 8310-GS) until 5 weeks of tumor growth in 100ml of PBS.

Tumor sizes for each experiment were measured every 2-4 days using digital calipers, and tumor volumes were calculated using the following formula: volume = $0.5 \times (\text{length} \times \text{width}^2)$. Mice were euthanized after 5 weeks or when a group reached 1500 mm^3, and tumor and lung tissue was preserved. Half of the tissue was embedded in paraffin and the other half was flash frozen and processed for protein analysis. All reagents injected in live mice were tested for endotoxin levels at University of Pennsylvania Cell Center Services using The Associates of Cape Cod LAL test.

Immunohistochemistry (IHC)

Mouse tumor and lung sections were paraffin embedded and sectioned. Paraffin embedded sections were rehydrated through a series of xylene and different concentrations of alcohol, which was followed with a rinse in water and washed in PBS. Slides were put with an antigen retrieval buffer (#3300, Vector Labs, Burlingame, CA) and steamed for 20 minutes. Slides were then blocked in a peroxide blocking buffer (#TA060H2O2Q, Thermo Scientific) for 15 minutes, followed by protein block (#TA-060-UB, Thermo Scientific) for 5 minutes and incubated with the primary antibody of interest which was prepared in antibody diluent (S0809, Dako). Slides were put in a humidified chamber at 4C overnight. Samples were washed with PBS and incubated in biotinylated anti-rabbit (#ab64256 Abcam), followed by streptavidin-HRP solution at room temperature for 20 minutes (#TS-060-HR Thermo Scientific). Samples were then washed with PBS and incubated with AEC (3-Amino-9Ethyl-l-Carboazole) chromogen for the appropriate amount of time after optimization (#TA060SA, Thermo Scientific). Slides were then washed with water and incubated in Mayer's hematoxylin (MHS1, Sigma) for 1 minute, rinsed with water, and mounted in Aquamount (#143905, Thermo Scientific). Lungs were assessed for localization of mCherry positive melanoma cells using a Nikon eclipse 80I digital. The number of mCherry cells per high power field (HPF) per lung section was assessed using automated NIS elements software and was analyzed using GraphPad Prism.

TCGA and CCLE Analysis

RNA-Seq of the TCGA and the Cancer Cell Line Encyclopedia (CCLE) data was downloaded from the TCGA database using cBioportal (http://www.cbioportal.org). Individual gene expression values for genes of interest were retrieved as normalized RNA-Seq by Expectation Maximization (RSEM) read counts processed through the TCGA and CCLE cBioportal. The data was then transformed to represent a standardized Z-score for each gene and further transformed such that genes of interest (Wnt5A, AXL, MER) were separated into two groups based on the top 25 percentile and bottom 25 percentile of gene expression within the melanoma patient samples from the TCGA dataset (N=~120) t and the top and bottom 50^{th} percentile for melanoma cells within the CCLE (N=~34). A students t-test (unpaired) was then performed on each gene in the data set to individually analyze the difference in average Z-score in low *vs.* high percentile melanoma samples. Data is presented as a heatmap based on high (red, 0.5) and low (blue, -0.5) z-scores and associated p-value. Significance was taken at $p<0.05$. Overall survival and progression free interval was obtained from the TCGA dataset. Metastatic patient samples only (Distant and lymph) were stratified into those that survived in under 3 years vs greater then 3 years and data was analyzed using a students T-test and present as the mean +/- SEM. Kaplan Meier probability/survival plots were also performed on metastatic patient samples.

Proteomics

Fibroblasts were plated at an equal number and grown to 70~ confluency in a 10 cm dish. They were washed one time with PBS and 5 times with serum free media, and then grown for 16 hours in 10 mls of serum free media. Conditioned media was collected, centrifuge at low speed to remove cells and debris, then centrifuge through a 0.22 um filter. Protease inhibitors (PMSF, Pepstatin A, and Leupeptin) were

added and samples at this time were flash frozen at -80 ^{o}C until ready. Fibroblasts from the 10cm dish were disassociated and cell number (haemocytometer) and protein concentration was determined using a Pierce BCA assay (Thermo Fisher). CM was then concentrated using a 3K MWCO ultrafiltration concentrator. Equal protein concentrations and media was assessed via colloidal Coomassie staining on a gel and BCA assay and proportional volumes were loaded on a preparative gel. Lanes for each sample were excised, digested with trypsin and analysed by TMT10plex with peptide fractionation. Raw protein intensity levels were log2 transformed and undetected intensities were floored to a minimum detected intensity across all proteins and samples. Unpaired students t-test was performed to estimate significance of difference between conditions and false discovery rate was estimated[33]. Proteins that passed FDR<5% were considered significant and top changed proteins with nominal p<0.05 were also reported on a scatter plot.

Statistical Analysis

For *in vitro* studies, a students t-test or Mann Whitney was performed for two-group comparisons. Estimate of variance was performed and unequal variances for the t-test were adjusted accordingly using Welch's correction. Multiple comparisons were performed using ANOVA or Kruskal-Wallis test with post-hoc Holm-Sidak's adjusted p-values. The indicated sample size for each *in vivo* study was designed to have 80% power at a two-sided alpha of 0.05 to detect a difference of large effect size of about 1.5 between two groups on a continuous measurement. GraphPad/Prism 8 was used for plotting graphs and statistical analysis. Significance was designated as follows: *, p<0.05; **, p<0.01; ***, p<0.001, p<0.0001, ****.

Declarations

Acknowledgements: We thank the outstanding Core Facilities of the Wistar Institute, supported by P30CA010815 and of the Johns Hopkins Kimmel Cancer Center, P30CA00697356; A.T. Weeraratna, S.M. Douglass, M. Fane, GM Alicea are supported by R01CA174746 and R01CA207935. GM Alicea and A.T. Weeraratna are also supported by P01 CA114046. M. Webster is supported by R00CA208012. HY. Tang is supported by R50CA221838. This work was supported in part by the Wistar Science Discovery Fund. AT Weeraratna is also supported by a Bloomberg Distinguished Professorship and the EV McCollum Endowed Chair.

Declaration of Conflicts

No financial conflicts or competing interests are declared.

References

1 Hoek, K. S. & Goding, C. R. Cancer stem cells versus phenotype-switching in melanoma. *Pigment Cell Melanoma Res***23**, 746-759, doi:10.1111/j.1755-148X.2010.00757.x (2010).

2 Fane, M. E., Chhabra, Y., Smith, A. G. & Sturm, R. A. BRN2, a POUerful driver of melanoma phenotype switching and metastasis. *Pigment Cell Melanoma Res*, doi:10.1111/pcmr.12710 (2018).

3 Kaur, A., Webster, M. R. & Weeraratna, A. T. In the Wnt-er of life: Wnt signalling in melanoma and ageing. *Br J Cancer***115**, 1273-1279, doi:10.1038/bjc.2016.332 (2016).

4 Kaur, A. *et al.* sFRP2 in the aged microenvironment drives melanoma metastasis and therapy resistance. *Nature***532**, 250-254, doi:10.1038/nature17392 (2016).

5 Webster, M. R. *et al.* Paradoxical Role for Wild-Type p53 in Driving Therapy Resistance in Melanoma. *Mol Cell*, doi:10.1016/j.molcel.2019.11.009 (2019).

6 Kaur, A. *et al.* Remodeling of the collagen matrix in aging skin promotes melanoma metastasis and affects immune cell motility. *Cancer Discov*, doi:10.1158/2159-8290.CD-18-0193 (2018).

7 Ecker, B. L. *et al.* Age-Related Changes in HAPLN1 Increase Lymphatic Permeability and Affect Routes of Melanoma Metastasis. *Cancer Discov*, doi:10.1158/2159-8290.CD-18-0168 (2018).

8 Alicea, G. M. *et al.* Changes in Aged Fibroblast Lipid Metabolism Induce Age-dependent Melanoma Cell Resistance to Targeted Therapy Via the Fatty Acid Transporter FATP2. *Cancer Discov*, doi:10.1158/2159-8290.CD-20-0329 (2020).

9 Pereira, C., Schaer, D. J., Bachli, E. B., Kurrer, M. O. & Schoedon, G. Wnt5A/CaMKII signaling contributes to the inflammatory response of macrophages and is a target for the antiinflammatory action of activated protein C and interleukin-10. *Arteriosclerosis Thrombosis and Vascular Biology***28**, 504-510, doi:10.1161/Atvbaha.107.157438 (2008).

10 Trevant, B. *et al.* Expression of secreted frizzled related protein 1, a Wnt antagonist, in brain, kidney, and skeleton is dispensable for normal embryonic development. *Journal of Cellular Physiology***217**, 113-126, doi:10.1002/jcp.21482 (2008).

11 Blakely, B. D. *et al.* Wnt5a Regulates Midbrain Dopaminergic Axon Growth and Guidance. *Plos One***6**, doi:ARTN e18373

10.1371/journal.pone.0018373 (2011).

12 Webster, M. R. *et al.* Wnt5A promotes an adaptive, senescent-like stress response, while continuing to drive invasion in melanoma cells. *Pigment Cell Melanoma Res***28**, 184-195, doi:10.1111/pcmr.12330 (2015).

13 Muller, J. *et al.* Low MITF/AXL ratio predicts early resistance to multiple targeted drugs in melanoma. *Nat Commun***5**, 5712, doi:10.1038/ncomms6712 (2014).

14 Tworkoski, K. A. *et al.* MERTK controls melanoma cell migration and survival and differentially regulates cell behavior relative to AXL. *Pigment Cell Melanoma Res***26**, 527-541, doi:10.1111/pcmr.12110 (2013).

15 Vardabasso, C. *et al.* Histone Variant H2A.Z.2 Mediates Proliferation and Drug Sensitivity of Malignant Melanoma. *Mol Cell***59**, 75-88, doi:10.1016/j.molcel.2015.05.009 (2015).

16 Ren, D. *et al.* Wnt5a induces and maintains prostate cancer cells dormancy in bone. *J Exp Med***216**, 428-449, doi:10.1084/jem.20180661 (2019).

17 Yumoto, K. *et al.* Axl is required for TGF-beta 2-induced dormancy of prostate cancer cells in the bone marrow. *Sci Rep-Uk***6**, doi:ARTN 36520

10.1038/srep36520 (2016).

18 Lambert, A. W., Pattabiraman, D. R. & Weinberg, R. A. Emerging Biological Principles of Metastasis. *Cell***168**, 670-691, doi:10.1016/j.cell.2016.11.037 (2017).

19 Sosa, M. S. *et al.* NR2F1 controls tumour cell dormancy via SOX9- and RARbeta-driven quiescence programmes. *Nat Commun***6**, 6170, doi:10.1038/ncomms7170 (2015).

20 Sosa, M. S., Bragado, P. & Aguirre-Ghiso, J. A. Mechanisms of disseminated cancer cell dormancy: an awakening field. *Nature Reviews Cancer***14**, 611, doi:10.1038/nrc3793 (2014).

21 Gao, X. L., Zhang, M., Tang, Y. L. & Liang, X. H. Cancer cell dormancy: mechanisms and implications of cancer recurrence and metastasis. *Onco Targets Ther***10**, 5219-5228, doi:10.2147/OTT.S140854 (2017).

22 Gomis, R. R. & Gawrzak, S. Tumor cell dormancy. *Mol Oncol*, doi:10.1016/j.molonc.2016.09.009 (2016).

23 Weeraratna, A. T. *et al.* Wnt5a signaling directly affects cell motility and invasion of metastatic melanoma. *Cancer Cell***1**, 279-288, doi:Doi 10.1016/S1535-6108(02)00045-4 (2002).

24 O'Connell, M. P. *et al.* Hypoxia induces phenotypic plasticity and therapy resistance in melanoma via the tyrosine kinase receptors ROR1 and ROR2. *Cancer Discov***3**, 1378-1393, doi:10.1158/2159-8290.CD-13-0005 (2013).

25 Raskin, L. *et al.* Transcriptome profiling identifies HMGA2 as a biomarker of melanoma progression and prognosis. *J Invest Dermatol***133**, 2585-2592, doi:10.1038/jid.2013.197 (2013).

26 Wellbrock, C. & Arozarena, I. Microphthalmia-associated transcription factor in melanoma development and MAP-kinase pathway targeted therapy. *Pigment Cell Melanoma Res***28**, 390-406, doi:10.1111/pcmr.12370 (2015).

27 Schoumacher, M. & Burbridge, M. Key Roles of AXL and MER Receptor Tyrosine Kinases in Resistance to Multiple Anticancer Therapies. *Curr Oncol Rep***19**, 19, doi:10.1007/s11912-017-0579-4 (2017).

28 Zhu, S. *et al.* A genomic screen identifies TYRO3 as a MITF regulator in melanoma. *Proc Natl Acad Sci U S A***106**, 17025-17030, doi:10.1073/pnas.0909292106 (2009).

29 Lew, E. D. *et al.* Differential TAM receptor-ligand-phospholipid interactions delimit differential TAM bioactivities. *Elife***3**, doi:10.7554/eLife.03385 (2014).

30 Davra, V., Kimani, S. G., Calianese, D. & Birge, R. B. Ligand Activation of TAM Family Receptors-Implications for Tumor Biology and Therapeutic Response. *Cancers (Basel)***8**, doi:10.3390/cancers8120107 (2016).

31 Lemke, G. Biology of the TAM receptors. *Cold Spring Harb Perspect Biol***5**, a009076, doi:10.1101/cshperspect.a009076 (2013).

32 Gomes, A. P. *et al.* Age-induced accumulation of methylmalonic acid promotes tumour progression. *Nature***585**, 283-287, doi:10.1038/s41586-020-2630-0 (2020).

33 Storey, J. D. & Tibshirani, R. Statistical significance for genomewide studies. *Proc Natl Acad Sci U S A***100**, 9440-9445, doi:10.1073/pnas.1530509100 (2003).

Figures

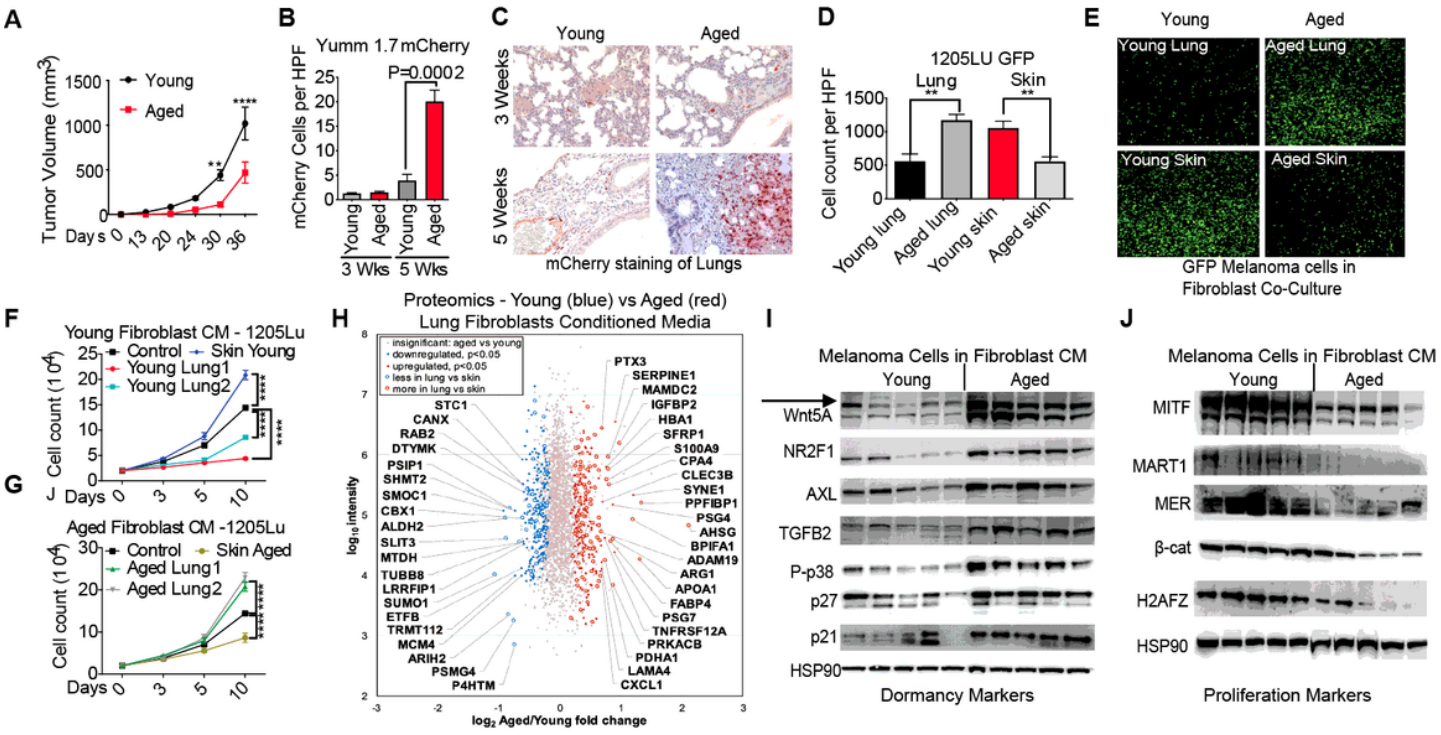

Figure 1

The aged lung microenvironment promotes efficient lung metastasis via aged fibroblasts. A Young (8 week) and aged (<52 week) c57BL6 mice were subdermally injected with 2.5x105 Yumm1.7 mCherry murine melanoma cells and tumors were measured over 36 days. N=5. B-C Lungs were collected and PFA embedded from tumor bearing young and aged mice at weeks 3 and 5 and IHC was performed using an mCherry antibody. Total number of positive cells were counted and averaged per high powered field (20x) and presented as mean +/- SEM, with representative images displayed (N=5). D-E Collagen sandwich reconstructs were formed with healthy human lung or skin fibroblasts from young (>35) or aged (<55) patients in the top and bottom layer. The middle layer contained 1205lu GFP human melanoma cells seeded at the same density on day 0. GFP positive melanoma cells were imaged using an automated Nikon TI and an average count per field was quantified using imaging software NIS elements at day 4. F-G 1205lu GFP melanoma cells were seeded at a density of 2x104. Cells were then grown over a 10 day period in conditioned media from young or aged lung or skin fibroblasts and underwent cell counting at days 3,5 and 10. H Proteomic analysis was performed on two combined young (>35) vs aged (<55) healthy human lung fibroblasts in triplicate. Unpaired t-test was performed to estimate significance of difference between conditions and false discovery rate was estimated. Proteins that passed FDR<5% were considered significant.I-J Western blot analysis was performed on tumor protein lysate from 5 young and 5 aged mice investigating dormancy and proliferative associated expression. HSP90 was used as a loading control.

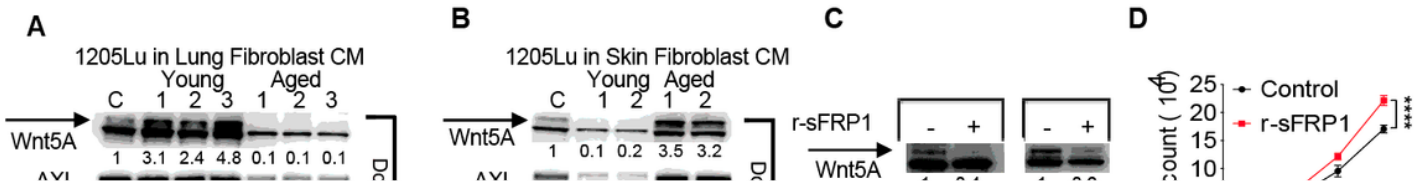

Figure 2

The aged lung fibroblast secretome promotes metastatic melanoma outgrowth via sFRP1 secretion. A-B Protein lysate was collected from 1205lu human melanoma cells treated with young or aged lung or skin fibroblast conditioned media over a 5-day period. Western blot analysis was performed examining dormant (Wnt5A, AXL, NR2F1, p21, p27 P-p38) and proliferative (H2AFZ, MER, MITF) melanoma markers. Densitometry analysis was performed relative to the loading control HSP90, and was normalized to control (C) cells. C Yumm1.7 and 1205lu melanoma cells were treated with recombinant sFRP1 every two days and protein expression was assessed after 5 days via western blot. D Proliferation was assessed in these cells over 10 days of treatment. E Aged-lung fibroblasts were transduced with lentiviral sh-sFRP1 (SH) or scrambled control (NEG) vectors. Westernblot analysis was performed on protein lysates. F Conditioned media (CM) was taken from SH and control (shNEG) fibroblasts after 72 hours. 1205lu melanoma cells were initially seeded at 2x104 and were grown in CM, or with regular media (DMEM) for 10 days with proliferation assessed. G-H Aged mice were subdermally injected with 2.5x105 Yumm1.7

mCherry melanoma cells. After three weeks of tumor growth, mice were treated with 1mg/kg of a neutralizing sFRP1 or an IgG control antibody via IP injection every 4 days and lung metastasis was assessed at week 5 via total number of positive cells averaged per high powered field (20x). Data was presented as mean +/- SEM, with representative images displayed (N=6). I Comparative diagram displaying key differences in the metastatic cascade between young and aged patients. A switch from sFRP2 to sFRP1 secretion by aged fibroblasts in the aged skin and lung respectively promotes efficient metastatic progression in aged models

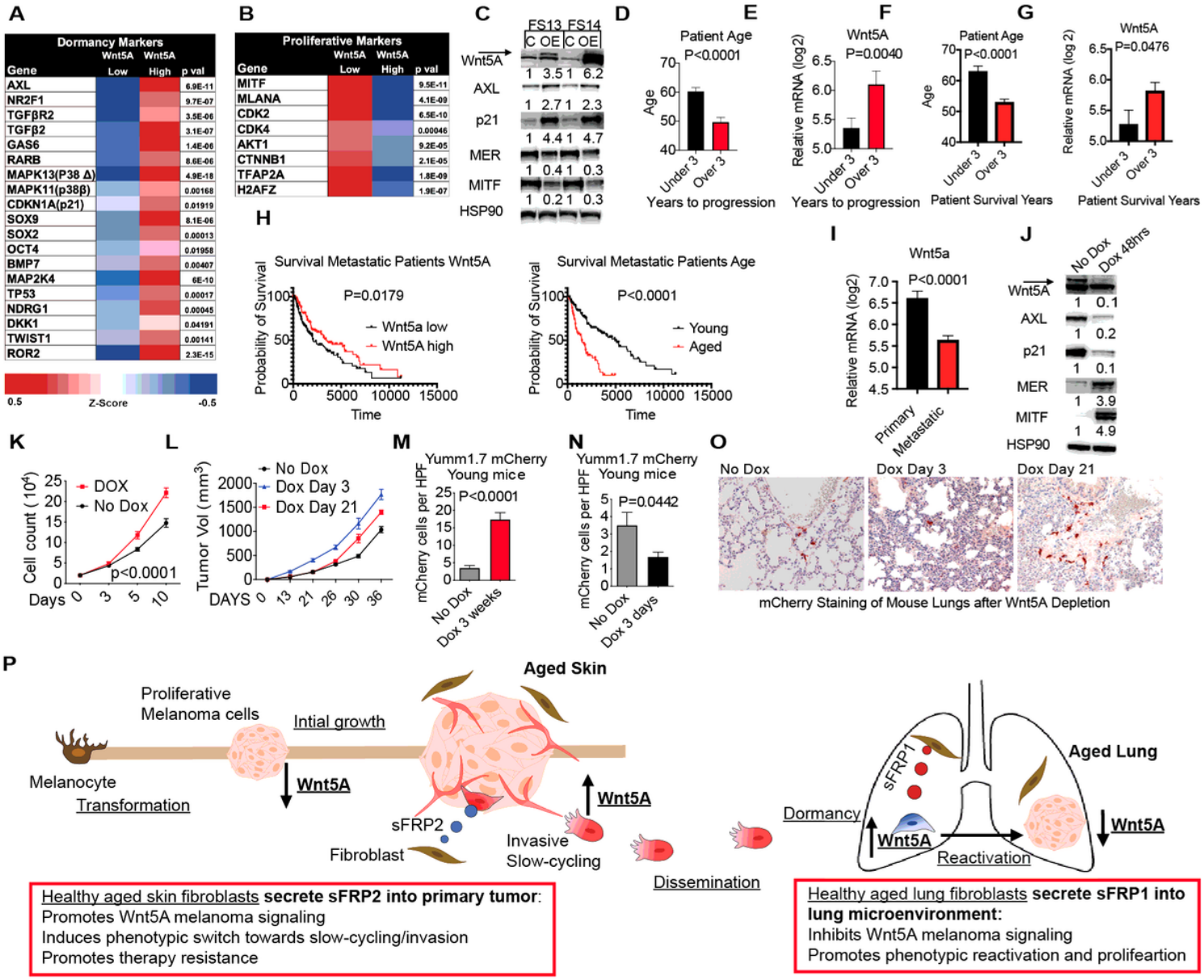

Figure 3

Temporal downregulation of Wnt5A promotes metastatic melanoma outgrowth in previously dormant microenvironments. A-B Analysis of the melanoma TCGA dataset (all samples) was performed on human samples stratified into the top (Wnt5A high) and bottom (Wnt5a low) 25th percentile of Wnt5A expression and presented as a heat map of the average Z-score. Unpaired t-test was performed to estimate

significance of difference between conditions and P<0.05 was considered significant. C Protein expression analysis was performed on Wnt5A low human melanoma samples (FS13, FS14) that underwent lentiviral induced overexpression of Wnt5A (OE). Densitometry was performed against HSP90, which was used as a loading control and values were normalized to control (C) for each line. D-E TCGA analysis was performed on metastatic (distant and lymph mets only) patient samples stratified by progression free index (PFI) for samples that progressed in under 3 years vs those that took longer than 3 years or did not progress. Patient age and relative Wnt5A mRNA expression was assessed. F-G TCGA analysis was performed as described looking at overall patient survival. H TCGA comparative Kaplan Meier analysis of probability of survial against total days in Wnt5A low vs Wnt5A high and young (under 55) vs aged (over 65) metastatic patients. (I) TCGA analysis of relative mRNA expression of Wnt5A in patient tumor samples comparing primary vs metastatic (distant and lymph mets) tissue sites. J Westernblot analysis was performed on Yumm1.7 doxycycline (DOX) inducible shWnt5A mCherry melanoma cells comparing control and DOX (0.5ug/ml) treated cells over 48 hours. Densitometry was performed against HSP90, which was used as a loading control and values were normalized to control. K Proliferation assay comparing DOX treated (0.5ug/ml) and control Yumm1.7 DOX inducible shWnt5A mCherry melanoma cells over a 10 day period. L Tumor volumes from young mice subdermally injected with 2.5x105 Yumm1.7 DOX inducible shWnt5A mCherry melanoma cells. Mice were treated with DOX (2ug/ml in water) from day 3 or day 21 onwards, with tumors measured for 5 weeks. M-O IHC analysis of mCherry positive melanoma cells in the lungs of these mice was assessed after 5 weeks of tumor growth via an average count per high powered field, with representative images displayed for each (N=6). Data was presented as mean +/- SEM. P Representative diagram of melanoma metastatic progression and dormancy reactivation in young vs aged patients, highlighting the complex nature of Wnt5A expression required at each metastatic timepoint.

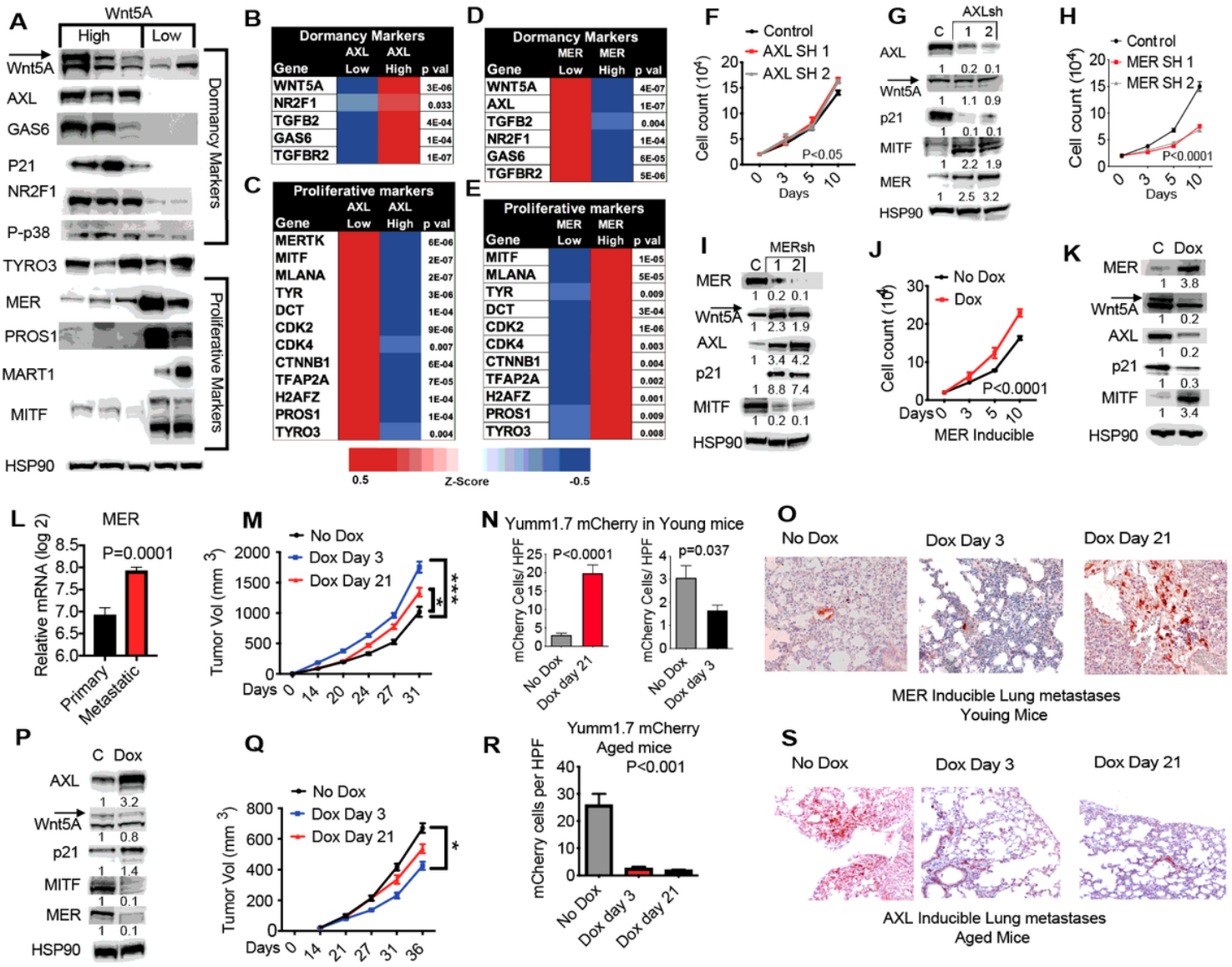

Figure 4

Age-induced differential AXL/MER axis promotes a dormancy and reactivation axis during metastatic melanoma. A Protein expression analysis of 3 Wnt5A high (FS4, FS5, 1205lu) and 2 Wnt5A low (FS13, FS14) human melanoma samples. HSP 90 was used as a loading control. B-C Analysis of melanoma cell lines from the Cancer Cell line Encyclopedia (CCLE) dataset was performed on human samples stratified into the top (AXL high) and bottom (AXL low) 50th percentile of MER expression (N=30) and presented as a heat map of the average Z-score. An unpaired t-test was performed on each condition, investigating previously established dormancy and proliferative genes, with P<0.05 considered significant. D-E Analysis of MER high and MER low cells from the CCLE as described. F 1205lu shAXL and control human melanoma cells were seeded at a density of 2x104. Cells were then grown over a 10-day period and proliferation was assessed. G Westernblot analysis was performed on these shAXL vs control lysates. Densitometry was performed against HSP90, which was used as a loading control and values were normalized to control (C) for each line H-I Proliferation assay and western blot assays as described on shMER FS13 and control human melanoma cells. J-K Western blot and proliferation assay as described

on Dox inducible MER Yumm1.7 melanoma cells vs non-dox control cells. L TCGA analysis of relative mRNA expression of MER in patient tumor samples comparing primary vs metastatic (distant and lymph mets) tissue sites. M Tumor volumes from young mice subdermally injected with 2.5x105 Yumm1.7 DOX inducible MER mCherry melanoma cells. Mice were treated with DOX (2ug/ml in water) from day 3 or day 21 onwards and compared with a no dox control and were measured over 31 days. N-O IHC analysis of mCherry positive melanoma cells in the lungs of these mice was assessed after 5 weeks of total tumor growth via an average count per high powered field, with representative images displayed for each (N=5). Data was presented as mean +/- SEM. P Western blot analysis of on Dox inducible AXL Yumm1.7 melanoma cells vs non-dox control cells. Q Tumor volumes from aged mice subdermally injected with 2.5x105 Yumm1.7 DOX inducible AXL mCherry melanoma cells. Mice were treated with DOX (2ug/ml in water) from day 3 or day 21 onwards and compared with a no dox control and were measured over 36 days. R-S IHC analysis of mCherry positive melanoma cells in the lungs of these mice as described above.

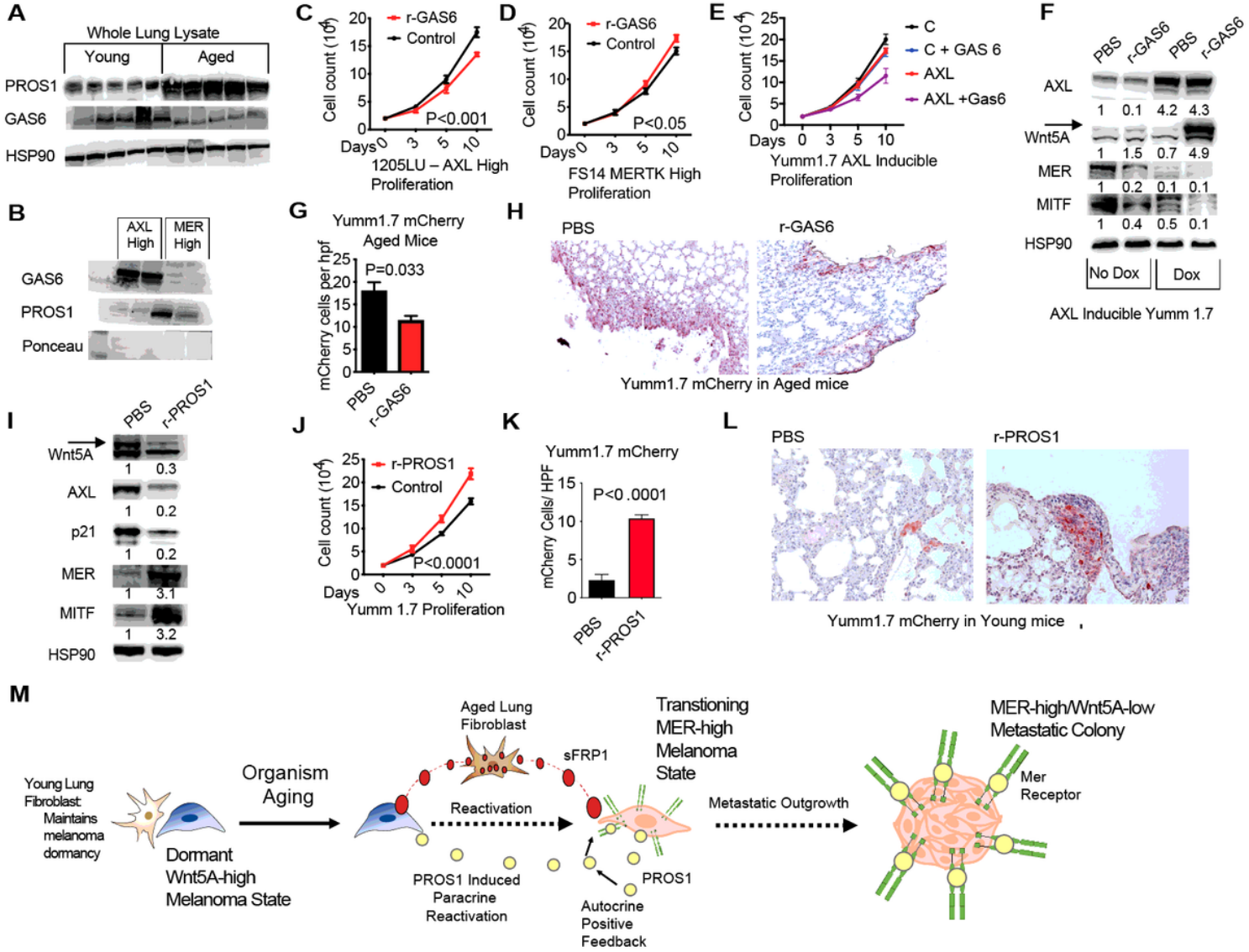

Figure 5

PROS1 promotes reactivation of dormant melanoma tumor cells in aged lung microenvironment. A Westernblot analysis of PROS1 and GAS6 in whole lung lysate from 5 young and 5 aged healthy mice. HSP90 was used as a loading control. B Westernblot analysis of 48 hour old condition media from 2 AXL high (FS4, 1205lu) and 2 MER high (FS13, FS14) human melanoma cells looking at PROS1 and GAS6. Initial protein expression was normalized via a BCA assay and a ponceau staining was performed as a loading control. C-D 1205lu and FS14 human melanoma cells were seeded at a density of 2x104. Cells were then grown over a 10-day period and treated with recombinant GAS6 and proliferation was assessed. E Proliferation assay as described above of Yumm1.7 AXL inducible cells treated with GAS6 or a PBS control in the presence or absence of DOX. F Westernblot analysis of lysates from Yumm1.7 AXL inducible cells described in E. G-H Aged mice were subdermally injected with 2.5x105 Yumm1.7 mCherry melanoma cells. After three weeks of tumor growth, mice were subsequently treated with rGAS6 or PBS via IP injection every 2 days and lung metastasis was assessed at week 5 via IHC analysis of the average count of mCherry positive melanoma cells per high powered field, with representative images displayed for each. Data was presented as mean +/- SEM. I Westernblot analysis as described of Yumm1.7 cells treated with recombinant PROS1. J Proliferation assay as described above of Yumm1.7 cells treated with recombinant PROS1. K-L Young mice were subdermally injected with 2.5x105 Yumm1.7 mCherry melanoma cells. After three weeks of tumor growth, mice were subsequently treated with PROS1 or PBS via IP injection every 2 days and lung metastasis was assessed at week 5 via IHC analysis of the average count of mCherry positive melanoma cells per high powered field, with representative images displayed for each. Data was presented as mean +/- SEM. M Diagram depicting aged induced metastatic reactivation from dormancy, centered around a sFRP1/PROS1 secreted ligand axis that promotes downregulation of Wnt5A/AXL mediated dormancy towards a MER proliferative reactivation state.